Supplementary Information (SI) for Journal of Materials Chemistry A.
This journal is © The Royal Society of Chemistry 2025

Supplementary information

A Ru-MoC heterostructure electrocatalyst for efficient and stable hydrogen oxidation reaction in alkaline media

*Pengcheng Wang,[†ab] Yang Yang,[†*b] Hongda Shi,[†b] Jiahe Yang,[b] Xingyan Chen,[b] Xi Lin,[b] Qianwang Chen[b] and Mingzai Wu[*ac]*

[a] School of Materials Science and Engineering, Hefei Institute of Technology, Hefei, 238076, China.

[b] Hefei National Research Center for Physical Sciences at the Microscale and Department of Materials Science and Engineering, University of Science and Technology of China, Hefei, 230026, China.

[c] Key Laboratory of Structure and Functional Regulation of Hybrid Materials, Ministry of Education, Institute of Energy, Hefei Comprehensive National Science Center, Anhui University, Hefei, 230601, China.

* Corresponding author, E-mail: yangyang1991@ustc.edu.cn , wumz@ahu.edu.cn.

† These authors contributed equally.

Experimental sections

Materials. Ammonium molybdate ($(NH_4)_6Mo_7O_{24}\cdot 4H_2O$), Ruthenium chloride hydrate ($RuCl_3\cdot nH_2O$), ammonium hydroxide ($NH_3\cdot H_2O$,28 wt.%), absolute ethyl alcohol(C_2H_5OH), Potassium hydroxide (KOH) were obtained from Sinopharm Chemical Reagent Co. Ltd (China). Dopamine hydrochloride($C_8H_{11}NO_2\cdot HCl$) was purchased from Aladdin chemical Ltd. Nafion (5 wt. %) were purchased from Sigma-Aldrich. Commercial Pt/C (20 wt. %) were purchased from Johnson Matthey. The deionized water was homemade in our lab. All the chemicals were firsthand to be utilized with no further treatment.

Synthesis of Mo-PDA. The Mo-MOF precursor (Mo-PDA) was prepared with a modified method basing on previous reports.[1] In a typical synthesis, 600 mg $(NH_4)_6Mo_7O_{24}\cdot 4H_2O$ and 600 mg dopamine hydrochloride were dispersed in 160 mL deionized water and 320 mL anhydrous ethanol, respectively, under vigorous stirring for 30 min to form uniform colorless transparent liquids. The solutions were then marked as solution A and solution B, respectively. Subsequently, solution B was slowly poured into solution A and the color of the solution becomes orange turbid. Then, 3 mL of $NH_3\cdot H_2O$ (28 wt.%) was injected into the above mixture solution and stirred for 6 h. Next, the orange precipitate (Mo-PDA) was collected by centrifugation and washed three time with ethanol, and dried in a vacuum oven at 60 ℃.

Synthesis of MoC/C. The as-synthesized Mo-PDA precursor was placed in a quartz boat and annealed at 800 ℃ for 3 h under a H_2 (5%) / Ar (95%) mixed flow with a heating rate of 3 ℃ min^{-1} to obtain the MoC/C composite.

Synthesis of Ru-MoC/C. 40 mg MoC/C was dispersed in 10 mL absolute ethyl alcohol under sonication for 30 min. Then 3 mL of 10 mg mL^{-1} $RuCl_3$ solution was added and stirred for 12 h. After that, the solvent was evaporated, then the obtained Ru^{3+}-MoC/C was dried at 60 °C for 10 min. Finally, the obtained powder was placed in a quartz boat and annealed at 300 ℃ for 90 min under a H_2 (5%) / Ar (95%) mixed flow with a heating rate of 5 ℃ min^{-1} to get the Ru-MoC/C.

Synthesis of Ru-MoO_2/C. The as-synthesized Mo-PDA precursor was placed in a quartz boat and annealed at 650 ℃ for 2 h under a H_2 (5%) / Ar (95%) mixed flow with a heating rate of 5 ℃ min^{-1} to obtain the MoO_2/C

composite. The Ru-MoO_2/C was prepared using the similar method with Ru-MoC/C except for replacing MoC/C with MoO_2/C.

Synthesis of Ru/C. The Ru/C was prepared using the similar method with Ru-MoC/C except for replacing MoC/C with carbon black (XC-72R).

Materials characterization

The powder X-ray diffraction (XRD) patterns of the samples were collected from a Japan Rigaku D/MAX-γA X-ray diffractometer equipped with Cu Kα radiation (λ=1.54178Å). Field emission scanning electron microscopy (FESEM) images were recorded on a JEOLJSM-6700 M scanning electron microscope. Transmission electron microscopy (TEM) images were recorded with a Hitachi H-7650 transmission electron microscope using an accelerating voltage of 200 kV, and high resolution transmission electron microscope (HRTEM) (JEOL-2011) was operated at an acceleration voltage of 200 kV. The specific surface area was evaluated at 77 K using the Brunauer-Emmett-Teller (BET) method (Micromeritic TriStar II 3020 V1.03 instrument), while the pore volume and pore size were calculated according to the Barrett-Joyner-Halenda (BJH) formula applied to the adsorption branch. Raman spectra were recorded with a Lab RAM HR Raman spectrometer. X-ray photoelectron spectroscopy (XPS) was conducted on an ESCALAB 250 X-ray photoelectron spectrometer instrument. Inductively coupled plasma-atomic emission pectrometer (ICP-AES) were conducted to determine the Ru and Mo concentrations of the samples with an Optima 7300 DV instrument. Ultraviolet photoemission spectroscopy (UPS) measurements were performed at the Catalysis and Surface Science End station (BL11U) of the National Synchrotron Radiation Laboratory (NSRL) in Hefei, China.

ICP test preprocessing.

In order to ensure that all Ru and Mo dissolved in aqua regia, we weighed a certain amount of electrocatalyst, put it in aqua regia and stirred it in the air, then let it stand for 30 min, transferred it to a high-pressure reactor and reacted at 180 ℃ for 12 h, and diluted aqua regia with a certain amount of deionized water after the reaction was complete and sufficiently cooled.

Preparation of working electrodes. Typically, 4 mg of catalyst was dispersed in a solution containing

970 μL of the ethanol solvent and 30 μL Nafion solution and ultrasonicated for at least 30 minutes to form a uniform catalyst ink. A total of 5 μL of well-dispersed catalyst ink was dripped onto the pre-polished GCE disk.

Electrocatalytic measurements details.

All electrochemical tests were carried out at CHI 760E electrochemistry workstation. The GCE loaded with electrocatalysts served as the working electrode, the platinum wire served as the counter electrode and the Ag/AgCl electrode served as reference electrode. In this work, all the measured potentials were referred to the reversible hydrogen electrode (RHE) potential. For HOR electrochemical test, 0.1 M KOH was used as the electrolyte.

Before HOR tests, cyclic voltammetry (CV) were conducted in H_2-saturated electrolyte to obtain the steady voltammetry curves. Then, polarization curves were recorded using a rotation disk electrode (RDE) with a rotation speed of 1600 rpm at a scan rate of 1 mV s^{-1} in H_2-saturated electrolyte for HOR. Electrochemical impedance spectra (EIS) tests were carried out after each RDE measurement. The real part of the resistance was used to obtain the iR-free potential for the potential data of HOR in this work.

AEMFCs test. The synthesized Ru-MoC/C catalyst or Ru/C catalyst was applied as the anode catalyst with a loading of 0.3 mg_{Ru} cm^{-2}. And the cathode catalyst was Pt/C (40 wt. % Pt) with a loading of 0.4 mg_{Pt} cm^{-2}. The hydroxide exchange membrane (PAP-TP-85) and ionomer (PAP-TP-100) were applied for $AEMFC_S$. The catalyst ink was prepared by ultrasonically dispersing the catalysts and ionomer into water and isopropanol (1:9 v/v) for 1 hour. Then the catalyst ink was sprayed onto both sides of the PAP-TP-85 membrane to fabricate a catalyst coated membrane (CCM) with the electrode area of 5 cm^2. The CCM was immersed into 3M KOH solution for 3 h for performance test and then rinsed thoroughly with deionized water to remove excess KOH. The rinsed CCM was assembled with a fluorinated ethylene propylene (FEP) gasket, a GDL (Sigracet SGL 29BC), a graphite bipolar plate with a 5 cm^2 flow field and a metal current collector for each side to complete the full fuel cell. A fuel cell test system (Scribner 850e) equipped with a back-pressure module was used for all the AEMFC tests. Test conditions: cell temperature of 92 °C, anode humidifier temperature of 82 °C, cathode

humidifier temperature of 86 °C, H_2 flow rate of 2.0 L min^{-1} and O_2 flow rate of 2.0 L min^{-1}. Backpressures were symmetric at 250 kPa.

Calculation of the HOR kinetic current density and exchange current density

The kinetic current (j_k) was calculated using the Koutecky-Levich equation:

$$\frac{1}{j} = \frac{1}{j_k} + \frac{1}{j_d} \qquad \textbf{Supplementary Equation (1)}$$

Where j is measured current and j_d is diffusion-limited current, which is obtained by Nernstian diffusional overpotential (η_d), assuming infinitely reaction kinetics:

$$\eta_d = -\frac{RT}{2F} \ln\left(1 - \frac{j_d}{j_l}\right) \qquad \textbf{Supplementary Equation (2)}$$

Where R is the universal gas constant, T is the temperature in Kelvin, F is Faraday's constant, j_l is the HOR limiting current.

The HOR exchange current (j_0) was obtained by micro-polarization method. In a small potential window of the micro-polarization region near the equilibrium potential (±5 mV vs. RHE), j_k approximately equals to the measured current j. In this case, the Butler–Volmer equation can be expanded by Taylor's formula and simplified as

$$j = j_0 \frac{\eta F}{RT} \qquad \textbf{Supplementary Equation (3)}$$

Therefore, j_0 can be obtained from the slope of the linear fitting in the micro-polarization region. The exchange current density (j_0) was normalized by the rotating disk electrode surface area.

Calculation details:

All the calculations were based on density functional theory by using the Vienna ab-initio simulation package (VASP).[1] The generalized gradient approximation (GGA) with the function of Perdew-Becke-Ernzerhof (PBE) was employed to describe the electron interaction energy of exchange correlation.[2] The projector augmented wave was applied to describe the electron-ion interaction and the plane-wave energy cutoff was set to 450 eV. The convergences of energy and force were set to 1×10^{-5} eV and 0.02eV/Å, respectively. Brillouin zone sampling was employed using a Monkhorst-Packing grid with 3 × 3 × 1 for structural optimization and 9 × 9 × 3 for energy self-consistent calculation.

The HBE were calculated by:

$$HBE = E_{*H} - E_{*} - 1/2\ E_{H2} \qquad (6)$$

The OHBE were calculated by:

$$OHBE = E_{*OH} - E_{*} - E_{OH} \qquad (7)$$

Where E_{*H} and E_{*OH} represent the energy of catalysts with the adsorbed H and OH species; while E_* and E_{H2} stand for the energies of the clean surface of catalysts and the H_2 molecules. As to the E_{OH}, it can be obtained by $E_{OH} = E_{H2O} - 1/2\ E_{H2}$.

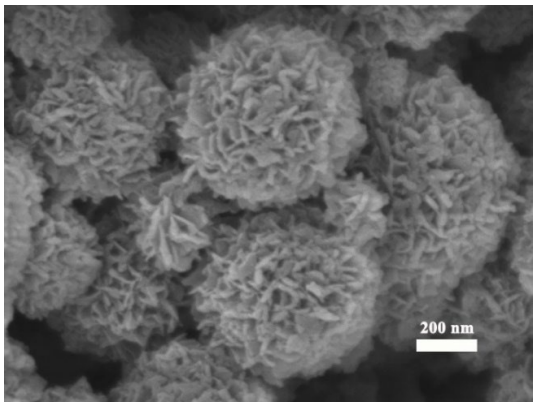

Figure S1. The SEM image of Mo-PDA.

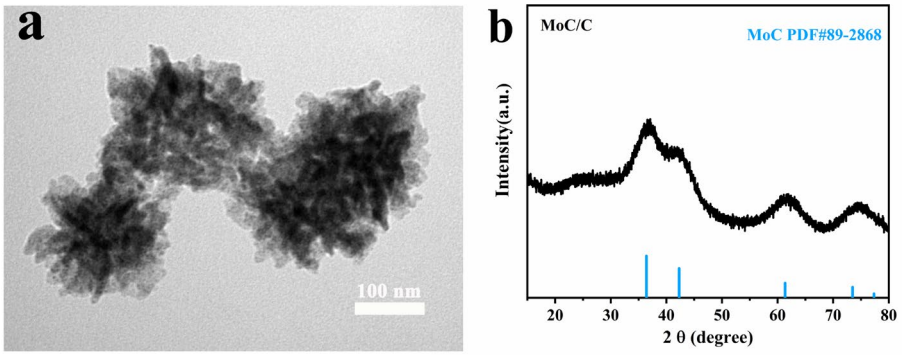

Figure S2. (a)The TEM image and (b) the XRD pattern of MoC/C.

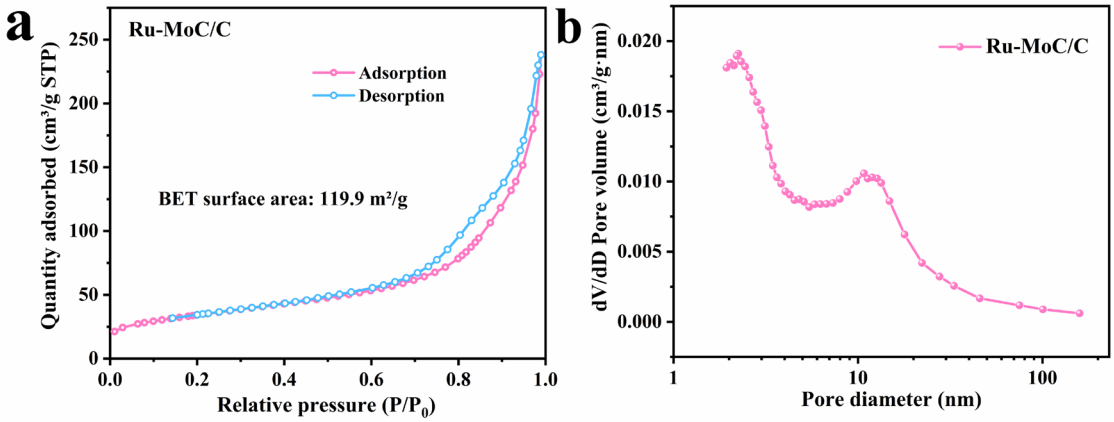

Figure S3. (a) N_2 adsorption and desorption isotherms and (b) pore size distribution curve of Ru-MoC/C

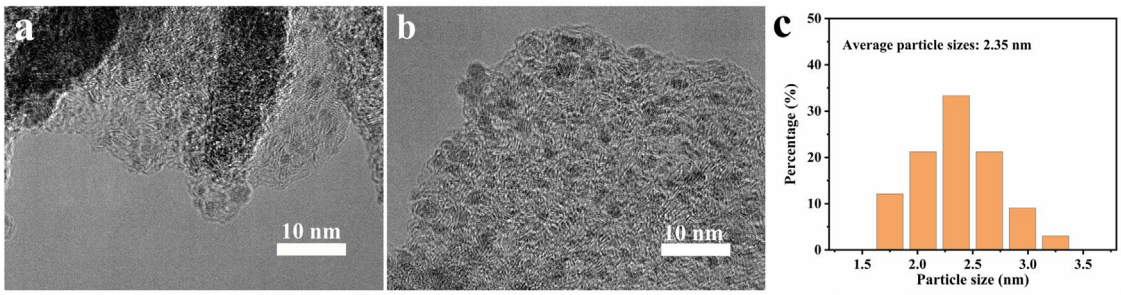

Figure S4. (a-b) HRTEM images of Ru-MoC/C with high magnification in different area, (c) particle size distribution of Ru-MoC/C based on Figure S4b.

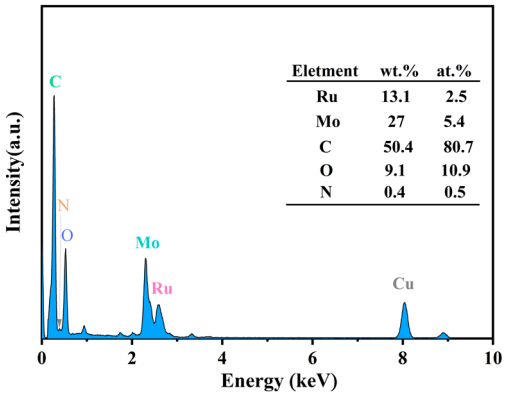

Eletment	wt.%	at.%
Ru	13.1	2.5
Mo	27	5.4
C	50.4	80.7
O	9.1	10.9
N	0.4	0.5

Figure S5. EDS spectrum of as-synthesized Ru-MoC/C.

Notes: EDS is mainly used to measure the metal element content on the surface of the sample. While ICP is mainly used to measure the metal element content of the whole sample. Therefore, we calculated the mass activity of catalysts according to ICP results.

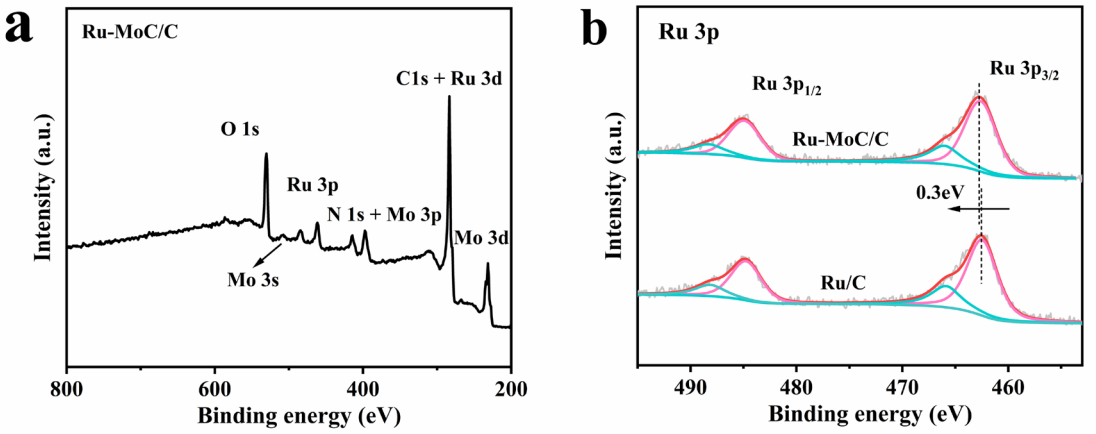

Figure S6. (a) XPS survey spectrum of Ru-MoC/C and (b) XPS spectra of Ru 3p for Ru-MoC/C and Ru/C.

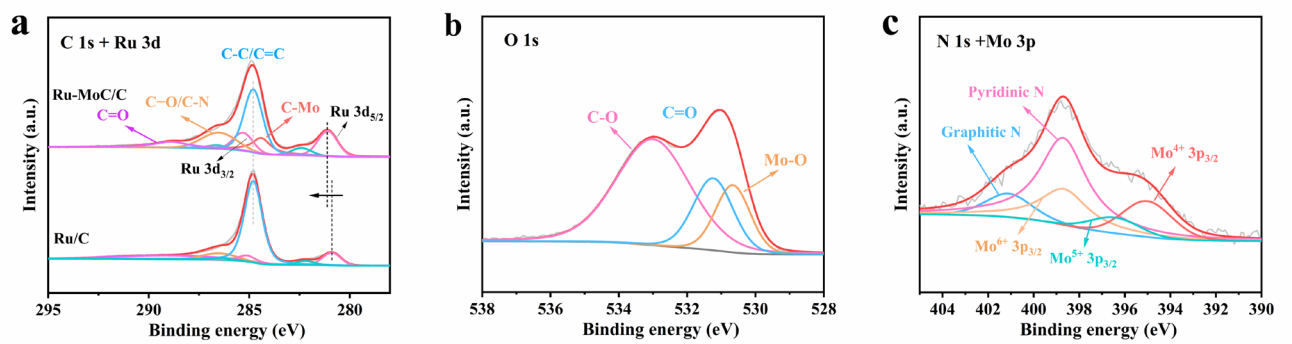

Figure S7. (a)The XPS spectra of C1s and Ru 3d for Ru-MoC/C and Ru/C, (b) O 1s XPS spectrum and (c) N1s and Mo 3p XPS spectra for Ru-MoC/C.

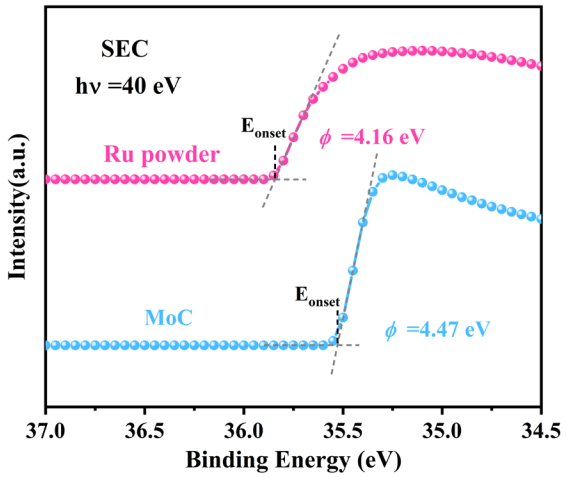

Figure S8. The UPS spectra of Ru powder and MoC.

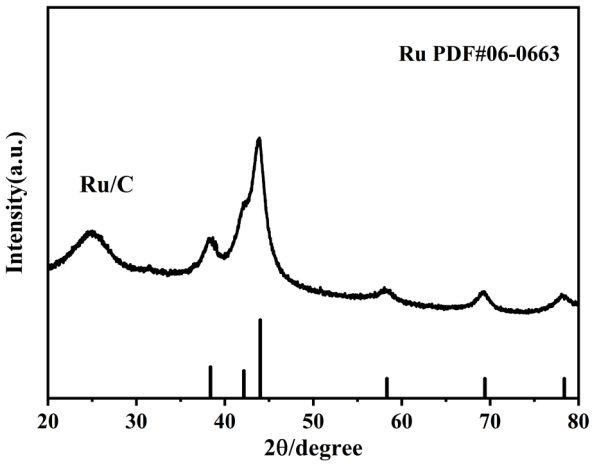

Figure S9. The XRD pattern of Ru/C.

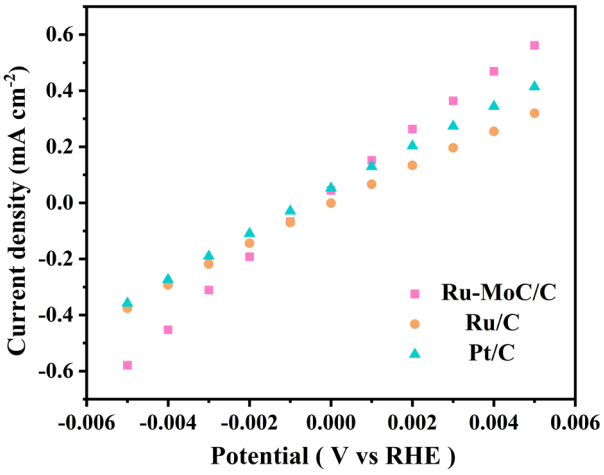

Figure S10. Linear-fitting curves in the micro-polarization region (-5 to 5 mV) of Ru-MoC/C, Ru/C, and commercial Pt/C, respectively.

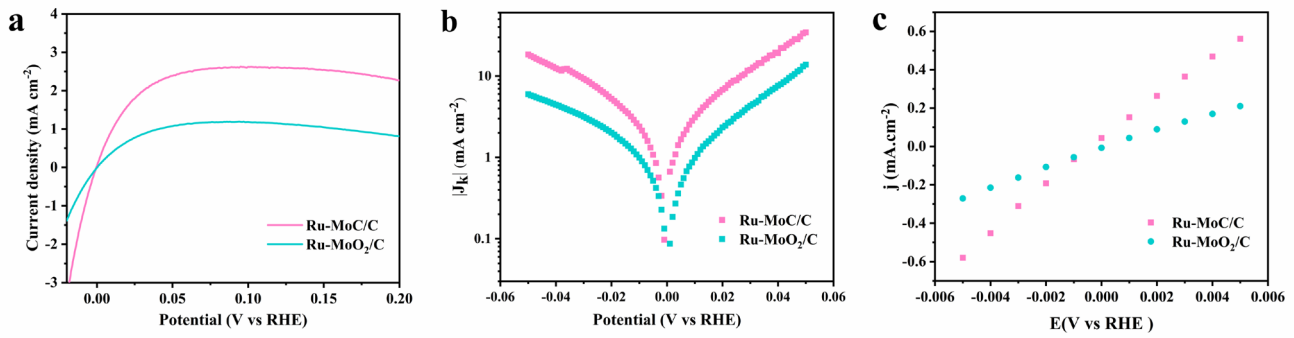

Figure S11. (a) HOR polarization curves in H_2 saturated 0.1 M KOH at a scan rate of 1 mV s^{-1} and rotation rate of 1600 rpm, (b) HOR Tafel plots of the kinetic current density and (c) Micro-polarization region (−5 to 5 mV vs RHE) of Ru-MoC/C and Ru-MoO_2/C, respectively.

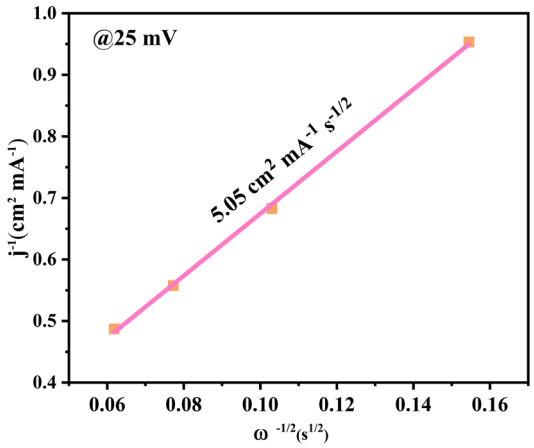

Figure S12. The Koutecky–Levich plot of Ru-MoC/C at an overpotential of 25 mV.

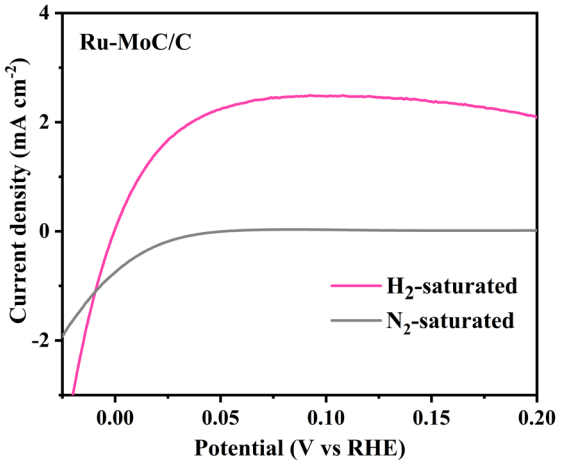

Figure S13. Polarization curves of Ru-MoC/C in H_2 and N_2 saturated 0.1 M KOH at a scan rate of 1 mV s^{-1} and rotation rate of 1600 rpm.

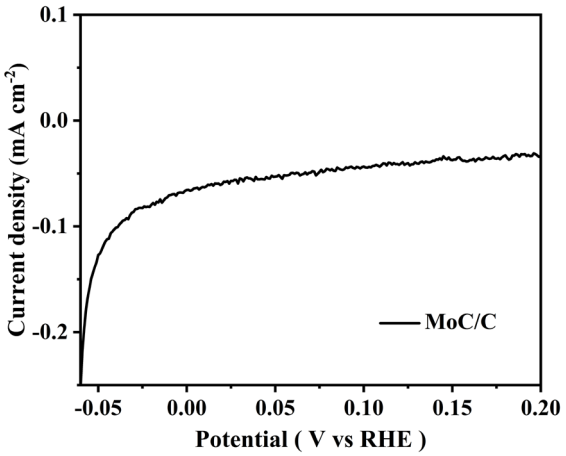

Figure S14. HOR polarization curve of MoC/C in H_2 saturated 0.1 M KOH at a scan rate of 1 mV s^{-1} and rotation rate of 1600 rpm.

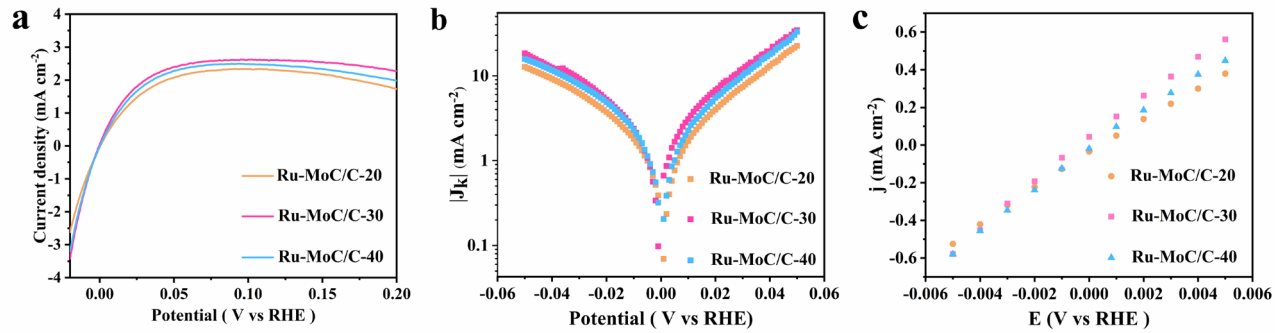

Figure S15. (a) HOR polarization curves in H_2 saturated 0.1 M KOH at a scan rate of 1 mV s^{-1} and rotation rate of 1600 rpm, (b) HOR Tafel plots of the kinetic current density and (c) Micro-polarization region (−5 to 5 mV vs RHE) of Ru-MoC/C-20, Ru-MoC/C-30 and Ru-MoC/C-40, respectively.

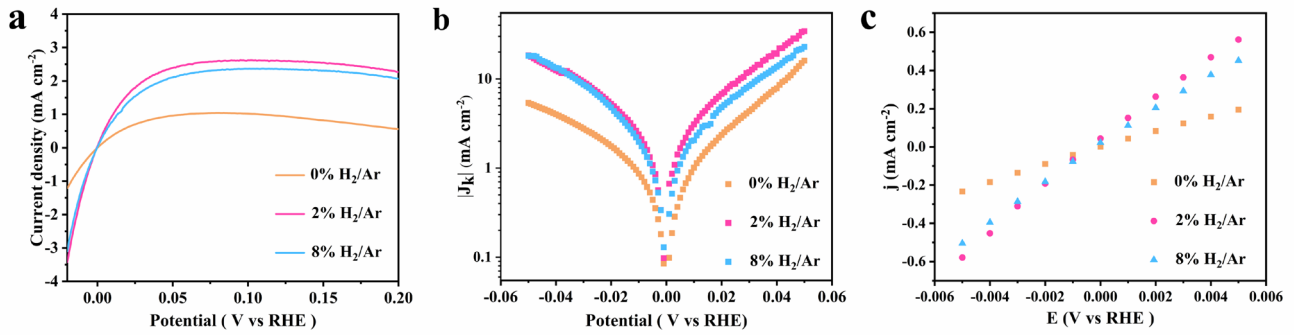

Figure S16. (a) HOR polarization curves in H_2 saturated 0.1 M KOH at a scan rate of 1 mV s^{-1} and rotation rate of 1600 rpm, (b) HOR Tafel plots of the kinetic current density and (c) Micro-polarization region (−5 to 5 mV vs RHE) of Ru-MoC/C obtained by being annealed in H_2/Ar mixed atmosphere with different ratio of H_2.

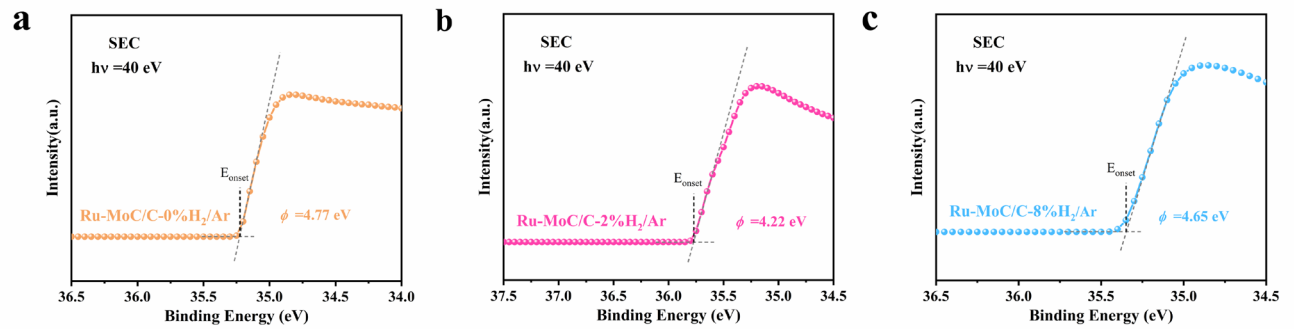

Figure S17. (a-c) The UPS spectra of the Ru-MoC/C obtained by being annealed in H_2/Ar mixed atmosphere with different ratio of H_2.

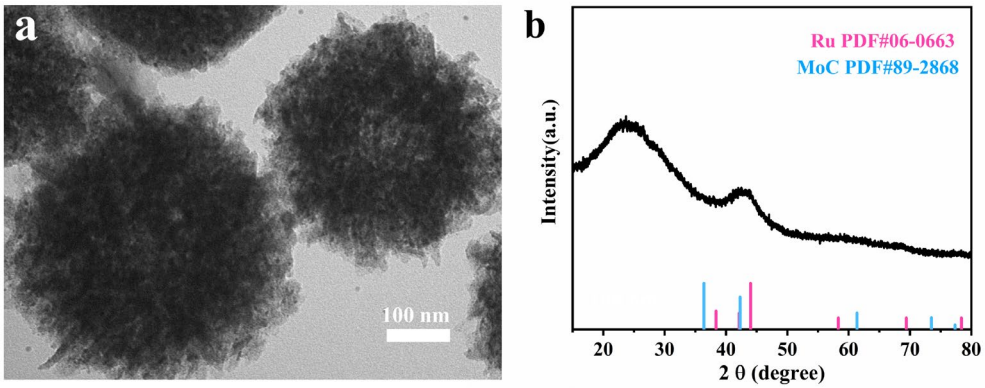

Figure S18. (a) TEM image and (b) XRD pattern of Ru-MoC/C after long-term stability test.

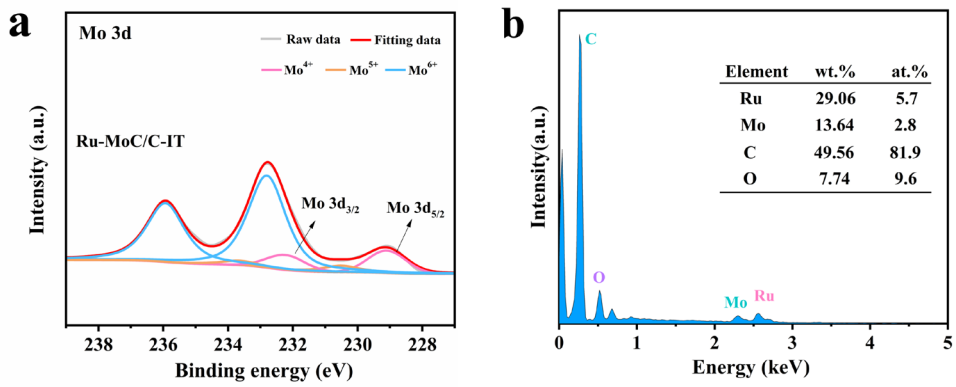

Figure S19. (a) XPS spectrum of Mo 3d and (b) EDS spectrum for Ru-MoC/C after long-term stability test.

Notes: the ratio of Mo^{4+} on the surface of Ru-MoC/C after stability test is decreased from 38.4% to 15.2%, while the ratio of Mo^{6+} on the surface of Ru-MoC/C after stability test is increased from 50.3% to 78.6%, indicating the surface of ultrasmall MoC nanoparticles was further oxidized during stability test. And EDS spectrum reveals that the content of Mo on the Ru-MoC/C surface is decreased, indicating the formed MoO_x on the MoC surface partially undergoes alkaline leaching.

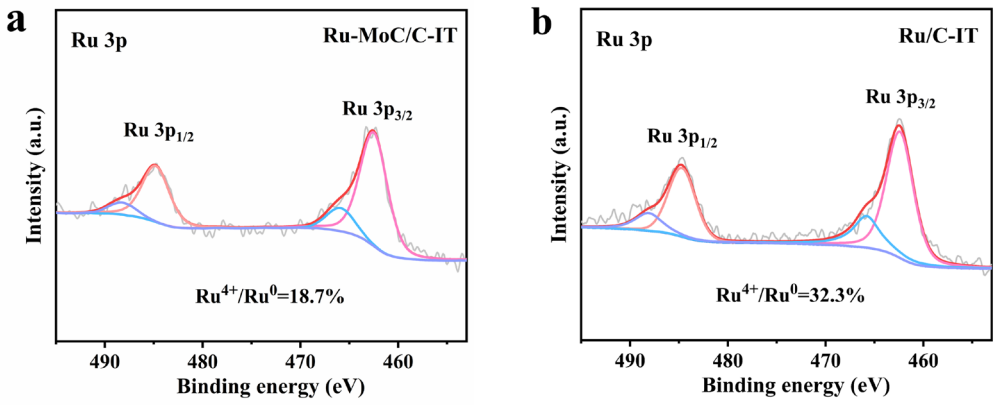

Figure S20. Ru 3p XPS spectra of (a) Ru-MoC/C and (b) Ru/C after long-term stability test.

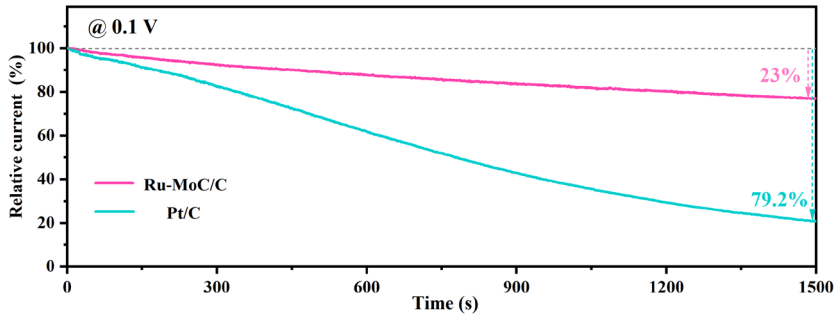

Figure S21. Relative current-time chronoamperometry response of Ru-MoC/C and Pt/C at 0.1 V vs RHE in H_2/1000 ppm CO-saturated 0.1 M KOH solutions.

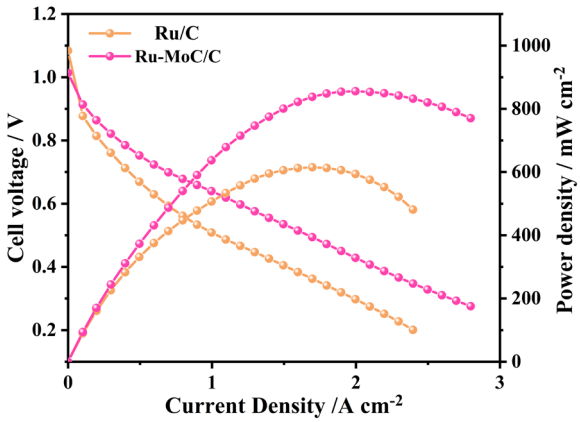

Figure S22. Polarization and power density curves of H_2/O_2 AEMFCs with Ru-MoC/C or Ru/C in the anode and Pt/C in the cathode. Test conditions: cell temperature at 92 °C, anode humidifier temperature at 82 °C and cathode humidifier temperature at 86 °C, H_2 flow rate at 2 L min^{-1} and O_2 flow rate at 2 L min^{-1}, and backpressures symmetric at 250 kPa.

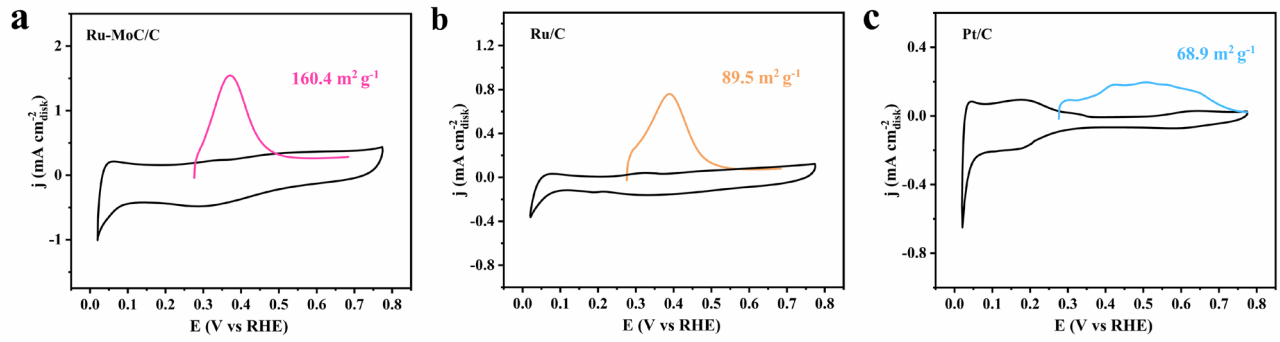

Figure S23. The Cu_{upd} stripping voltammogram in 0.5 M H_2SO_4 with 5 mM of $CuSO_4$ on (a) Ru-MoC/C; (b) Ru/C and (c)Pt/C.

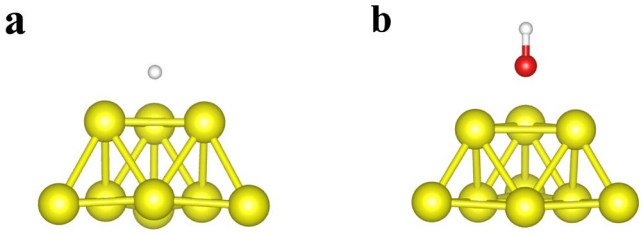

Figure S24. Optimized structures of (a) H*and (b) OH* adsorbed on Ru cluster models.

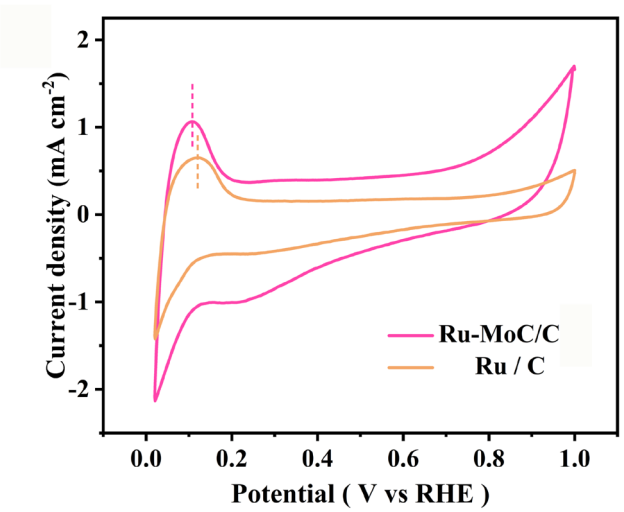

Figure S25. CVs curves of Ru/VOC and Ru/C in N_2-saturated 0.1M KOH solution at a scan rate of 20 mV s^{-1}.

Table S1. The results of ICP-AES for Ru-MoC/C and Ru/C.

Sample	Ru ($_{wt.}$ %)	Mo ($_{wt.}$ %)
Ru-MoC/C (Ru-MoC/C-30)	19.4	27.1
Ru/C	23.5	\

Table S2. Summary of mass activities and exchange current density for studied catalysts

Catalysts	Loading (μg_{metal} cm^{-2}_{disk})	Mass activities (mA μg^{-1}_{metal})	Exchange current density (mA cm^{-2})	ECSA (m^2 g^{-1})	Specific activities (mA cm^{-2}_{PGM})
Ru-MoC/C	19.8	1.74	2.93	160.4	0.092
Ru/C	24.0	0.43	1.78	89.5	0.083
Pt/C	20.4	0.57	1.99	68.9	0.141

Table S3. Comparison of HOR activities of reported Ru-based catalysts and this work.

Catalysts	Loading (μg_{metal} cm^{-2}_{disk})	Mass activities (mA μg^{-1}_{metal})	Ref
Ru-MoC/C	18.47	1.76	This work
IO-Ru–TiO_2/C	25.48	0.907	[3]
Ru/PEI-XC	21.7	0.423	[4]
Ru NP/PC	50.1	0.263	[5]
RuS_{2-x}	4.31	1.43	[6]
fcc-RuCrW	10.45	1.12	[7]
RuCr-2/C	4.5	0.568	[8]
$RuFe_{0.1}$/C	1.25	0.908	[9]
Ru-Ru_2P/C	8.33	1.256	[10]
Sub-2 nm Ru/HC	14.7	0.30	[11]
Ru_3Sn_7/C	7.05	0.658	[12]
hcp/fcc-Ru	6.57	1.016	[13]
Ru@C-340	10	1.2	[14]
Ni1Ru1/C	12.5	0.224	[15]
$CoRuSn(OH)_x$	/	3.89	[16]

Table S4. The actual contents in Ru in samples with different amount of $RuCl_3$ added.

Sample	Amount of $RuCl_3$	Ru ($_{wt.}$ %)
Ru-MoC/C-20	20 mg	13.3
Ru-MoC/C-30	30 mg	19.4
Ru-MoC/C-40	40 mg	20.5

Notes: the Ru-MoC/C-30 was named as Ru-MoC/C in this article.

References

(1) Kresse, G.; Hafner, J. Ab initio molecular dynamics for open-shell transition metals. *Phys Rev B* **1993**, *48* (17), 13115-13118.

(2) Perdew, J. P.; Burke, K.; Ernzerhof, M. Generalized Gradient Approximation Made Simple. *Phys. Rev. Lett.* **1996**, *77*, 3865-3868.

(3) Jiang, J.; Tao, S.; He, Q.; Wang, J.; Zhou, Y.; Xie, Z.; Ding, W.; Wei, Z. Interphase-oxidized ruthenium metal with half-filled d-orbitals for hydrogen oxidation in an alkaline solution. *J. Mater. Chem. A* **2020**, *8*, 10168-10174.

(4) Wang, J.; Liu, J.; Zhang, B.; Gao, J.; Liu, G.; Cui, X.; Liu, J.; Jiang, L. Amine-ligand modulated ruthenium nanoclusters as a superior bi-functional hydrogen electrocatalyst in alkaline media. *J. Mater. Chem. A* **2021**, *9*, 22934-22942.

(5) Ming, M.; Zhang, Y.; He, C.; Zhao, L.; Niu, S.; Fan, G. Y.; Hu, J. S. Room-Temperature Sustainable Synthesis of Selected Platinum Group Metal (PGM = Ir, Rh, and Ru) Nanocatalysts Well-Dispersed on Porous

Carbon for Efficient Hydrogen Evolution and Oxidation. *Small* **2019**, *15*, 1903057.
(6) Yang, C.; Yue, J.; Wang, G.; Luo, W. Activating and Identifying the Active Site of RuS_2 for Alkaline Hydrogen Oxidation Electrocatalysis. *Angew. Chem. Int. Ed.* **2024**, e202401453.
(7) Yue, J.; Li, Y.; Yang, C.; Luo, W. Hydroxyl-Binding Induced Hydrogen Bond Network Connectivity on Ru-based Catalysts for Efficient Alkaline Hydrogen Oxidation Electrocatalysis. *Angew. Chem. Int. Ed.* **2025,** 64, e202415447.
(8) Yang, C.; Li, Y.; Ge, C.; Jiang, W.; Cheng, G.; Zhuang, L.; Luo, W. The role of hydroxide binding energy in alkaline hydrogen oxidation reaction kinetics on RuCr nanosheet. *Chin. J. Chem.* **2022**, *40*, 2495-2501.
(9) Li, Y.; Yang, C.; Ge, C.; Yao, N.; Yin, J.; Jiang, W.; Cong, H.; Cheng, G.; Luo, W.; Zhuang, L. Electronic modulation of Ru nanosheet by d–d orbital coupling for enhanced hydrogen oxidation reaction in alkaline electrolytes. *Small* **2022**, *18*, 2202404.
(10) Su, L.; Jin, Y.; Gong, D.; Ge, X.; Zhang, W.; Fan, X.; Luo, W. The role of discrepant reactive intermediates on Ru-Ru_2P heterostructure for pH-universal hydrogen oxidation reaction. *Angew. Chem. Int. Ed.* **2022**, *63*, 202215585.
(11) Ma, M.; Chen, C.; Zhang, X.; Zhao, H.; Wang, Q.; Du, G.; Xie, Z.; Kuang, Q. Mo-modified electronic effect on Sub-2 nm Ru catalyst for enhancing the hydrogen oxidation catalysis. *J. Mater. Chem. A* **2023**, *11*, 10807–10812.
(12) Su, L.; Fan, X.; Jin, Y.; Cong, H.; Luo, W. Hydroxyl-binding energy-induced kinetic gap narrowing between acidic and alkaline hydrogen oxidation reaction on intermetallic Ru_3Sn_7 catalyst. *Small* **2023**, *19*, 2207603.
(13) Li, Y.; Yang, C.; Yue, J.; Cong, H.; Luo, W. Polymorphism-interface-induced work function regulating on Ru nanocatalyst for enhanced alkaline hydrogen oxidation reaction. *Adv. Funct. Mater.* **2023**, *33*, 2211586.
(14) Yang, Z.; Lai, W.; He, B.; Wang, J.; Yu, F.; Liu, Q.; Liu, M.; Zhang, S.; Ding, W.; Lin, Z.; et al. Tailoring Interfacial Chemistry of Defective Carbon-Supported Ru Catalyst Toward Efficient and CO-Tolerant Alkaline Hydrogen Oxidation Reaction. *Adv. Energy. Mater* **2023**, *13*,2300881.
(15) Liu, J.; Wang, J.; Fo, Y.; Zhang, B. Y.; Molochas, C.; Gao, J.; Li, W. Z.; Cui, X. J.; Zhou, X.; Jiang, L. H.; et al. Engineering of unique Ni-Ru nano-twins for highly active and robust bifunctional hydrogen oxidation and hydrogen evolution electrocatalysis. *Chem. Eng. J.* **2023**, *454*,139959.
(16) Liu, S.; Wang, X.; Huang, W.-H.; Zhang, Q.; Han, J.; Zhang, Y.; Pao, C.-W.; Hu, Z.; Xu, Y.; Huang, X., Solvation Effect-Determined Mechanisms of Cation Exchange Reactions for Efficient Multicomponent Nanocatalysts. *Angew. Chem. Int. Ed.* **2025**, *64*, e202418248.